

applied optics

Spectral 3D reconstruction of impressionist oil paintings based on macroscopic OCT imaging

XINGYU ZHOU,¹ DARLENE IN,² XING CHEN,² HEATHER McCune Bruhn,³ XUAN LIU,^{1,4} AND YI YANG^{2,5} (1)

¹Department of Electrical and Computer Engineering, New Jersey Institute of Technology, University Heights, Newark, New Jersey 07102, USA

Received 11 February 2020; revised 18 April 2020; accepted 22 April 2020; posted 23 April 2020 (Doc. ID 390326); published 20 May 2020

Art conservators have adopted optical technologies to improve conservation efforts; laser triangulation, stereophotogrammetry, structured light, laser scanners, and time of flight sensors have been deployed to capture the 3D information of sculptures and architectures. Optical coherence tomography (OCT) has introduced new imaging methods to study the surface features and subsurface structures of delicate cultural heritage objects. However, the field of view of OCT severely limits the scanning area. We present a hybrid scanning platform combined with an effective algorithm for real-time sampling and artifact removal to achieve macroscopic OCT (macro-OCT) imaging and spectral 3D reconstruction of impressionist style oil paintings. © 2020 Optical Society of America

https://doi.org/10.1364/AO.390326

1. INTRODUCTION

Art conservators routinely examine heritage works to determine their state of deterioration. Microscopic examination is one of the common routines that involves obtaining small samples of a painting or mural and assessing the sample under a microscope. Art conservators have adopted optical technologies to improve conservation efforts; laser triangulation, stereophotogrammetry, structured light, laser scanners, and time of flight sensors have been deployed to capture the 3D information of sculptures [1–3] and architectures [4]. 3D scanning devices have been used on paintings for art conservation efforts: 3D data collected based on conoscopic micro-profilometry/holography [5-7] has been integrated with 2D data to improve the conservation strategy [8,9]; a 3D range camera based on optical triangulation with fringe pattern projection was used to capture the 3D surface profile of "Adoration of the Magi" by Leonardo da Vinci at the Uffizi Gallery in Florence for conservation monitoring [10]; the famous painting "Mona Lisa" was 3D scanned with a high-resolution color laser scanner [11] based on trigonometry to generate the 3D coordinates, while simultaneously capturing the spectral information of the object; and more recent research has applied terahertz reflectometry to generate the surface profile and the cross-sectional information of paintings [12,13], which enables conservators to evaluate the layer structure of paintings. Other methods such as x-ray computer tomography and magnetic resonance imaging have been applied for cross-sectional imaging; however, these methods lack of spatial resolution for microscopic examinations [14,15].

The unique capabilities of optical coherence tomography (OCT) [16] have introduced new imaging methods to the field of cultural heritage conservation. OCT is a non-invasive imaging technique that acquires depth-resolved signals with micrometer resolution, which is highly advantageous in studying the surface features and subsurface structures of delicate cultural heritage objects [17,18] such as historical oil paintings and murals. Researchers have applied OCT to capture high-density (HD) cross-sectional information of paintings to reveal the layer structure [19,20], which is used for varnish layer and structural analysis [21] and varnish thickness determination [22,23]. Other applications such as identifying layer structure of ancient murals [24] and non-invasive monitoring of the varnish removal from easel paintings [25] have been demonstrated.

Despite these advantages, the small field-of-view (FOV) [26] of an OCT system severely limits its potential to cover a mesoscale or macroscopic region of interest (ROI) on a painting. In our previous study on OCT examination of paintings [27], we presented a proof of concept scanning system that performed raster scanning using a pair of galvanometers, and extended the lateral FOV by translating the sample painting using a pair of linear motors. The increased FOV image is then obtained by digitally stitching imagines from each step. However, galvanometers generally have higher resolution and accuracy than

²Division of Science and Engineering, Penn State Abington, 1600 Woodland Rd., Abington, Pennsylvania 19001, USA

³Department of Art History, Penn State, 240 Borland Building, University Park, Pennsylvania 16802, USA

⁴e-mail: xuan.liu@njit.edu

⁵e-mail: yzy1@psu.edu

linear motors. Therefore, the linear motors' translation error accumulated through each step introduced redundant sampling that resulted in artifacts in the image.

In this paper, we describe a hybrid scanning platform combined with effective algorithm for real-time sampling artifact removal to achieve macroscopic OCT (macro-OCT) imaging. The system enables large FOV, HD examination and 3D spectral reconstruction of the surface topography of paintings. The rest of the paper is organized as the follows: we describe the imaging platform and data acquisition protocol, demonstrate the spectral 3D reconstruction of an impressionist style oil painting, and finally conclude the paper with discussions.

2. SYSTEM

A. System Configuration

The macro-OCT imaging system is illustrated in Fig. 1. We use a swept source OCT (SS OCT) system for 3D imaging. The SS-OCT system (Axsun) operates at 1.06 µm with 100 nm bandwidth, 100 kHz Ascan rate. The output of the swept source illuminates a fiber-optic Michelson interferometer. A lens is used in the sample arm (Thorlabs LSM04-BB) to focus the probing beam and collect photons backscattered from the sample. Sample light interferes with reference light and the interferometric signal is detected. A frame grabber (PCIe-1433, National Instrument) acquires the data and streams the data to a host computer for image reconstruction and analysis. The computer uses a GPU (NVIDIA gtx1080) for parallel signal processing. The hybrid scanning platform consists of two parts to achieve large FOV OCT imaging. The first part of the scanning platform is the galvo system that uses two galvanometers (Thorlabs GVS002) to steer the incident light beam in the x and y directions for lateral scanning. The lateral FOV is determined by galvo scanning in the x and y directions. FOV_x and FOV_{y} are proportional to the focal length of the imaging objective ($F_{\text{obj}} = 54 \text{ mm}$ for the objective lens we used), the responsive factor of the galvanometer deflection angle to voltage (β) , and the voltage applied to the galvanometer $(V_x \text{ and }$ V_{γ}): FOV_x = $2\beta V_x F_{\text{obj}}$ and FOV_{γ} = $2\beta V_{\gamma} F_{\text{obj}}$. The second part of the hybrid scanning platform is a pair of linear stages used to increase the FOV of OCT imaging without compromising spatial resolution. The XYZ gantry linear stage was

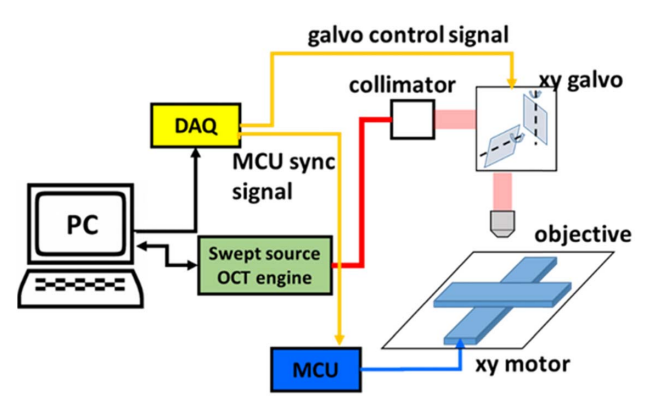


Fig. 1. Configuration of macro-OCT based on a hybrid scanning platform.

purchased from Intellidrives (Intellidrives X1-BEMA-W45-600). The control of the *X* and *Y* stages is integrated into the OCT imaging system. The *X* and *Y* stages have a translation resolution of 18.75 um. As illustrated in Fig. 1, a workstation computer (Dell Precision 5530) is used to coordinate and synchronize different modules of the macro-OCT system. The C++ program that synchronizes the data acquisition card (DAQ, National Instruments NI 6212) with galvo scanning is developed in-house. Meanwhile, we use a microcontroller unit (Arduino UNO REV3) to control the *XYZ* motion of the gantry linear stage and develop in-house software to sync the *XY* motion of the linear stage to the DAQ. Macroscopic FOV is achieved by synchronizing translational movements with iterating volumetric data acquisition.

B. Lateral Scanning and Data Acquisition Protocol for Macro-OCT Imaging

Lateral scanning for the macro-OCT imaging is illustrated in Fig. 2. The macro-OCT system first performs conventional volumetric data acquisition with the sample located at lateral coordinate (x_1, y_1) . By synchronizing data acquisition with galvo scanning, the imaging system obtains volumetric OCT data from an area represented by the rectangle shaded in blue, denoted as ROI₁. ROI₁ centers at (x_1, y_1) with x dimension of FOV_x and y dimension of FOV_y . When the OCT engine performs data acquisition from ROI₁, the linear motors remain still. After data acquisition is completed, the DAQ sends a trigger signal to the MCU. Upon receiving the trigger signal, the MCU moves the motor in the x dimension and/or in the γ dimension to a new lateral coordinate (x_2, y_2) . When the linear stage motion is complete, the OCT engine resumes volumetric data acquisition from the new area (ROI2) centered at (x_2, y_2) . This is again followed by linear motor translation. The process of data acquisition and motor translation repeats for N times. N sets of volumetric OCT data are obtained at $(x_1, y_1), (x_2, y_2), (x_3, y_3), ...,$ and (x_N, y_N) . For Fig. 2, N = n * p, where n is 10, and p is 9. These lateral coordinates are predefined, and the scanning pathway is shown in Fig. 2.

C. Image Stitching Methods

A redundant scanning strategy is adopted to ensure every point on the lateral plane of the sample is scanned for OCT imaging. In other words, there is overlapping between adjacent scanning areas for each linear stage position. Therefore, as shown in Fig. 2,

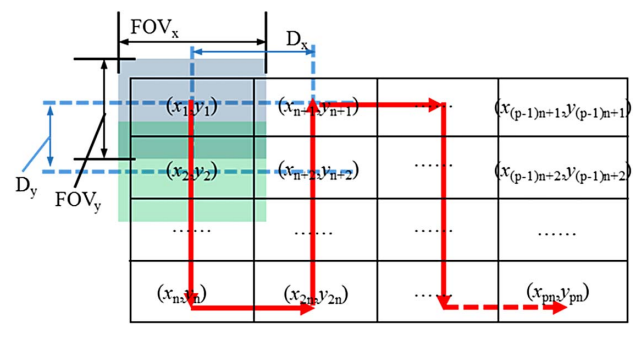


Fig. 2. Lateral scanning for macro-OCT imaging.

 $D_x < {\rm FOV}_x$ and $D_y < {\rm FOV}_y$, where D_x and D_y are the translation step sizes in the X and Y directions for the linear stage. Such a redundant scanning strategy is needed since galvanometers are highly linear and accurate (1.5 μ m scanning resolution) while the linear motors used to translate the sample have a lower translational resolution (18.75 μ m). The theoretical overlapping width is set to 300 um. However, the redundancy in data acquisition introduces image artifacts when volumetric OCT datasets are stitched together directly. To obtain an artifact-free OCT image with large FOV, we implement a method based on cross-correlation analysis to adaptively stitch S_0 , S_1 , ..., and S_{N-1} , where $S_k \in R^{Nx \times Ny \times Nz}$ are volumetric OCT datasets obtained with the sample located at (x_k, y_k) . In our previous study, a similar method was developed and validated to generate distortion-free OCT images using a manually scanned single fiber probe [28].

Consider imaging system acquired two adjacent volumetric OCT datasets of S_k and S_{k+1} . To digitally align the acquired data, we first reduce 3D datasets S_k and S_{k+1} to 2D by averaging pixel values along the axial dimension (z). The resultant datasets are denoted as M_k and M_{k+1} ($M_k \in \mathbb{R}^{Nx \times Ny}$ and $M_{k+1} \in \mathbb{R}^{Nx \times Ny}$), as shown in Figs. 3(a) and 3(b) (actual enface OCT image). If S_k and S_{k+1} are stitched together directly, as shown in Fig. 3(c), the same region (areas enclosed by the dashed rectangular boxes) will appear twice in the post-stitching image, resulting in image artifact. To remove artifacts due to redundant OCT scanning, we select a submatrix from the bottom of M_k , denoted as m_h , that contains a few numbers of rows [h rows within the rectangular box at the bottom of Fig. 3(a)]. We then sift through the second image (M_{k+1}), and determine a submatrix within M_{k+1} that best matches m_k . To achieve this, we select a submatrix from M_{k+1} , denoted as m_{k+1} , that contains h rows of data from M_{k+1} [subimage within the rectangular box at the top of Fig. 3(b)]. We calculate the Pearson correlation coefficient between m_k and m_{k+1} using Eq (1), where E() represents the expectation value, • represents the element-wise product, and $\sigma_{\boldsymbol{v}}$ represents the standard deviation of \boldsymbol{v} . The value of ρ is closer to 1 when m_k and m_{k+1} are extremely similar and decreases as

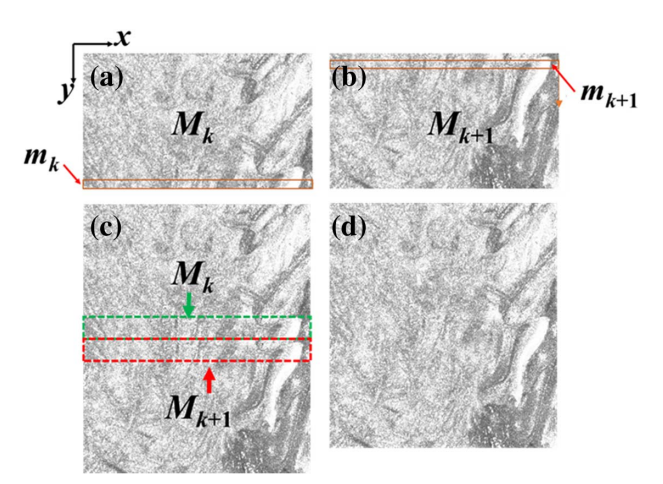


Fig. 3. Illustration of image stitching strategy. (a) An enface OCT image of the oil painting; (b) an enface OCT image of the oil painting with the sample translated in the *y* direction; (c) images directly stitched together with redundant artifact; (d) images stitched together through cross-correlation analysis after redundant artifact removal.

the similarity between m_k and m_{k+1} decreases. We use a window sliding along the y direction to select \mathbf{m}_{k+1} that consists of the wth to the (w+h-1)th row of \mathbf{M}_{k+1} , calculate a set of ρ , and determine the \mathbf{w} that corresponds to the largest ρ . We will attach data of \mathbf{M}_{k+1} to \mathbf{M}_k , starting from the wth Bscan, resulting in an artifact-free image [Fig. 3(d)]. The same data stitching strategy applies to every set of OCT data and we chose m_k and m_{k+1} to have five rows:

$$\rho = \frac{E[(m_k - \bar{m}_k) \cdot (m_{k+1} - \bar{m}_{k+1})]}{\sigma_{m_k} \sigma_{m_{k+1}}}.$$
 (1)

After stitching the dataset in the y direction, a similar approach is utilized to stitch images in the x direction.

3. RESULTS

In this study, we performed a macro-OCT imaging study on the oil painting produced by an artist that mimics the impressionist style. This oil on canvas painting is of 10 cm by 10 cm in size, shown in Fig. 4. We chose the impressionist style for its unique brushstrokes to demonstrate the 3D reconstruction capability of the optical imaging system.

We first applied conventional volumetric data acquisition using the OCT imaging system to acquire the volumetric dataset, and the FOV is indicated as a solid red box as shown in Fig. 4. The Ascan, Bscan, enface image, and 3D rendered volume of this area are shown in Figs. 5(a)-5(d). The Ascan obtained from the oil painting [Fig. 5(a)] indicates the depth penetration of the OCT signal. The Bscan [Fig. 5(b)] shows clear visible speckle patterns due to the high-density OCT imaging, which illustrates the surface profile variation, and can be used for subsurface layer structure analysis. The enface image in Fig. 5(c) was obtained by averaging pixel values along the axial dimension z. Figure 5(d) demonstrates the rendered surface topography of the paint in this area (solid red box in Fig. 4).

We further demonstrated the macro-OCT's capability for large FOV, HD OCT imaging to reconstruct the 3D surface profile of the painting. We used the motor system to translate the sample to different lateral coordinates following the data acquisition protocol shown in Fig. 2 (n = 10 and p = 9). We acquired 90 OCT images (about 100 KB for each image) at



Fig. 4. Sample painting. Oil on canvas, 10 cm by 10 cm. The dimension of the ROI (dotted line) is 27 mm by 18 mm. The dimension of the OCT FOV (solid line) is 3.8 mm by 2.3 mm.

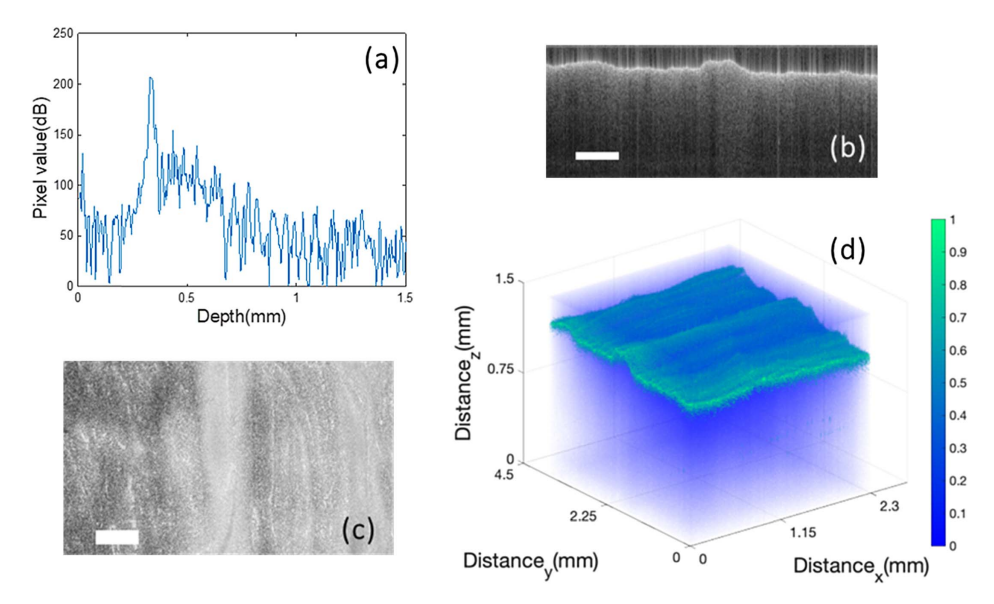


Fig. 5. (a) Ascan, (b) Bscan OCT image, (c) enface image, (d) 3D rendered volume. In (b) and (c), scale bar = 0.5 mm.

different transverse coordinates. A 27 mm by 18 mm transverse FOV was achieved to scan the ROI (dotted line in Fig. 4). Each 3D OCT data cube takes 5 s to acquire and every position transition takes 5 s. The total data acquisition time to scan the macroscopic FOV is about 900 s. The methods described in Section 2.C are used to digitally stitch the images together to minimize artifacts. The stitching process takes 60 s, and the stitched image has a size of 8 MB. The total size of the final stitched dataset depends on the size of the ROI and the size of each volumetric OCT scan. In this study, we are interested in the surface topography, and thus only the surface layers of the OCT data are acquired and stitched. This reduces the computational time and memory required to store the data. The enface image obtained by averaging OCT data along the axial dimension z is shown Fig. 6(a) where the scale bar represents 5 mm. To effectively visualize 3D characteristics of the 3D OCT dataset with macroscopic transverse FOV, we performed peak detection for each Ascan to identify the surface location in the axial dimension. Figure 6(b) shows the surface topography information in gray scale. There are noticeable vertical lines in Fig. 6(b). Figure 6(b) represents the surface topography of the scanned ROI. However, as the OCT scanner mechanically moves from one vertical position to the next one, a small global axial shift is introduced between different OCT data cubes due to mechanical error. The current algorithm performs image stitching and artifact removal using enface OCT images. As a result, the vertical lines representing small surface peak difference along

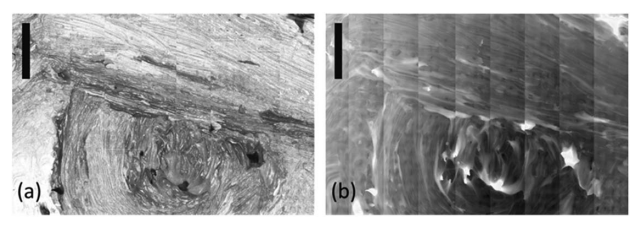


Fig. 6. (a) Stitched enface image of the ROI; (b) stitched surface topography of ROI. Scale bar = 5 mm.

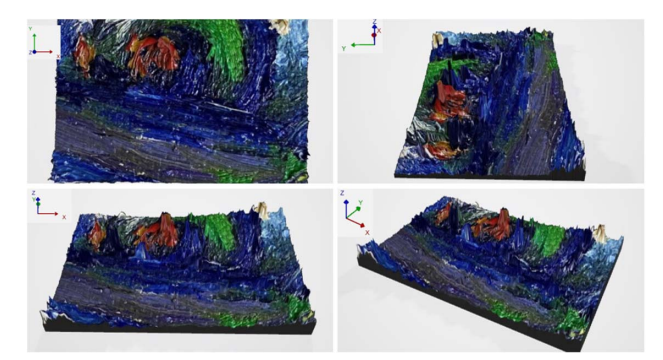


Fig. 7. Spectral and texture of the ROI from the impressionist oil painting.

each vertical scan cannot be removed using the current stitching algorithm. To eliminate the vertical lines in Fig. 6(b), surface peak adjustment has to be performed or the mechanical distance calibration between the sample and the OCT scanner has to be improved.

Finally, we projected the color image onto the surface topography dataset using 3D plug-in software (3D map generator) from Adobe Photoshop. The software first generates a 3D topography model via a gray-scale height image, and in this case from Fig. 6(b). Then we captured the 2D spectral image of the ROI. The software projects the 2D spectral image onto the 3D topography model and transforms it into the 3D spectral reconstruction of the ROI, containing both spectral and texture information. Figure 7 presents the spectral 3D reconstruction of the ROI on the painting (white dotted area in Fig. 4).

4. CONCLUSION

We have designed a hybrid scanning platform for macroscopic OCT to achieve spectral 3D reconstruction of delicate art works and potentially other cultural objects. Due to the OCT system's limited focal distance, the painting's maximum surface height

variation is 1.5 mm. This surface variation range is adequate for Old Master paintings and some impressionist paintings. However, an adaptive distance control mechanism, such as the OCT-based surface topology and motion compensation system [29], can be added to the OCT scanner to increase the system's surface height variation tolerance.

By using enface images acquired in each scan and stitching all of them with the method mentioned in Section 2.C, we can achieve high-resolution OCT imaging with increased FOV. This type of digital copy could serve as a backup method to capture the best possible details of art works to hedge against the worst-case scenario, such as war, terrorism, natural disaster, heist, and other catastrophes that put art works in vulnerable positions.

We further carried out customer discovery interviews to better understand the real-world applications and the need for the proposed system. We interviewed 25 potential users, namely an artist, a museum administrator, art historians and educators, and conservators. We have identified three potential applications of the digital reconstruction products. The 3D surface model of paintings can be used in classes to enhance art viewing experiences, especially for online courses. Students will be able to rotate, zoom in and out to view details of art works such as brushstrokes, and learn about various painting styles. 3D printed painting samples can be used to assist visually impaired users to experience various painting techniques, such as Van Gogh's brushstrokes and Pointillism demonstrated by Seurat's works. The OCT provides a minimally invasive method to generate the cross-sectional information of paintings, which can be used for art conservation work.

Funding. Samuel H. Kress Foundation; National Science Foundation Penn State I-Corps Site; Penn State University; and New Jersey Institute of Technology.

Acknowledgment. Dr. Kristin deGhetaldi and Prof. Brian Baade of University of Delaware provided critical advice on art conservation methods. Both Dr. DeGhetaldi and Mr. Baade have substantial experience working as art conservators in teaching and practicing. The painting sample is produced by Kali Wallace, who is a New Jersey based artist. She received her BFA and BA in art history from William Paterson University. She is current pursuing her MFA at Guizhou Minzu University, China. She is experienced in various painting styles and materials. She was recognized as 2014 New Jersey Visual Artist of the Year by RAW.

Disclosures. The authors declare no conflicts of interest.

REFERENCES

- G. Godin, J.-A. Beraldin, J. Taylor, L. Cournoyer, M. Rioux, S. El-Hakim, R. Baribeau, F. Blais, P. Boulanger, J. Domey, and M. Picard, "Active optical 3D imaging for heritage applications," IEEE Comput. Graph. Appl. 22, 24–36 (2002).
- M. Pieraccini, G. Guidi, and C. Atzeni, "3D digitizing of cultural heritage," J. Cult. Herit. 2, 63–70 (2001).
- P. S. Fowles, J. H. Larson, C. Dean, and M. Solajic, "The laser recording and virtual restoration of a wooden sculpture of Buddha," J. Cult. Herit. 4, 367s–371s (2003).

- N. Yastikli, "Documentation of cultural heritage using digital photogrammetry and laser scanning," J. Cult. Herit. 8, 423–427 (2007).
- N. Gaburro, G. Marchioro, and C. Daffara, "A versatile optical profilometer based on conoscopic holography sensors for acquisition of specular and diffusive surfaces in artworks," Proc. SPIE 10331, 48–56 (2017).
- G. Y. Sirat, "Conoscopic holography. I. Basic principles and physical basis," J. Opt. Soc. Am. A 9, 70–83 (1992).
- I. Alvarez, J. M. Enguita, M. Frade, J. Marina, and G. Ojea, "On-line metrology with conoscopic holography: beyond triangulation," Sensors 9, 7021–7037 (2009).
- R. Fontana, M. C. Gambino, M. Greco, L. Marras, E. M. Pampaloni, A. Pelagotti, L. Pezzati, and P. Poggi, "2D imaging and 3D sensing data acquisition and mutual registration for painting conservation," Videometrics VIII 5665, p. 51 (2005).
- R. Fontana, M. C. Gambino, M. Greco, L. Marras, M. Materazzi, E. Pampaloni, L. Pezzati, and P. Poggi, "Integrating 2D and 3D data for diagnostics of panel paintings," Proc. SPIE 5146, 88–98 (2003).
- G. Guidi, C. Atzeni, and S. Lazzari, "3D optical scanning diagnostics for Leonardo Da Vinci's," in *Proceedings of the Fourth International* Conference on 3-D Digital Imaging and Modeling, 2003(2003), pp. 110–115.
- M. L. Story, F. Blais, L. Cournoyer, J. Beraldin, and M. Picard, "3D imaging from theory to practice: the 3D imaging from theory to practice: the Mona Lisa story," Opt. Eng. 7060, 1–10 (2008).
- J. Dong, A. Locquet, M. Melis, and D. S. Citrin, "Global mapping of stratigraphy of an old-master painting using sparsity-based terahertz reflectometry," Sci. Rep. 7, 1–12 (2017).
- C. L. Koch Dandolo, M. Lopez, K. Fukunaga, Y. Ueno, R. Pillay, D. Giovannacci, Y. Le Du, X. Bai, M. Menu, and V. Detalle, "Toward a multimodal fusion of layered cultural object images: complementarity of optical coherence tomography and terahertz time-domain imaging in the heritage field," Appl. Opt. 58, 1281–1290 (2019).
- M. Schreiner, B. Frühmann, D. Jembrih-Simbürger, and R. Linke, "X-rays in art and archaeology: An overview," Powder Diffr. 19, 3–11 (2004).
- D. N. H. Notman, J. Tashjian, A. C. Aufderheide, O. W. Cass, O. C. Shane, T. H. Berquist, J. E. Gray, and E. Gedgaudas, "Modern imaging and endoscopic biopsy techniques in Egyptian mummies," Am. J. Roentgenol. 146, 93–96 (1986).
- C. S. Cheung, J. M. O. Daniel, M. Tokurakawa, W. A. Clarkson, and H. Liang, "High resolution Fourier domain optical coherence tomography in the 2 μm wavelength range using a broadband supercontinuum source," Opt. Express 23, 1992–2001 (2015).
- P. Targowski, B. Rouba, M. Wojtkowski, and A. Kowalczyk, "The application of optical coherence tomography to non-destructive examination of museum objects," Stud. Conserv. 49, 107–114 (2004)
- P. Targowski and M. Iwanicka, "Optical coherence tomography: Its role in the non-invasive structural examination and conservation of cultural heritage objects-a review," Appl. Phys. A 106, 265–277 (2012).
- P. Targowski, M. Iwanicka, M. Sylwestrzak, C. Frosinini, J. Striova, and R. Fontana, "Using optical coherence tomography to reveal the hidden history of the Landsdowne Virgin of the Yarnwinder by Leonardo da Vinci and Studio," Angew. Chemie—Int. Ed. 57, 7396–7400 (2018).
- H. Liang, M. Cid, R. Cucu, G. Dobre, A. Podoleanu, J. Pedro, and D. Saunders, "En-face optical coherence tomography—a novel application of non-invasive imaging to art conservation," Opt. Express 13, 6133–6144 (2005).
- P. Targowski, M. Góra, and M. Wojtkowski, "Optical coherence tomography for artwork diagnostics," Laser Chem. 2006, 1–11 (2006)
- T. Arecchi, M. Bellini, C. Corsi, R. Fontana, M. Materazzi, L. Pezzati, and A. Tortora, "A new tool for painting diagnostics: Optical coherence tomography," Opt. Spectrosc. 101, 23–26 (2006).
- I. Gorczynska, M. Wojtkowski, M. Szkulmowski, T. Bajraszewski, B. Rouba, A. Kowalczyk, and P. Targowski, "Varnish thickness determination by spectral optical coherence tomography," in *Lasers Conserv. Artworks* (Springer, 2007), pp. 493–497.

- 24. H. Liang, R. Lange, H. Howard, and J. Spooner, "Non-invasive investigations of a wall painting using optical coherence tomography and hyperspectral imaging," Proc. SPIE 8084, 80840F (2011).
- 25. M. Iwanicka, P. Moretti, S. van Oudheusden, M. Sylwestrzak, L. Cartechini, K. J. van den Berg, P. Targowski, and C. Miliani, "Complementary use of optical coherence tomography (OCT) and reflection FTIR spectroscopy for in-situ non-invasive monitoring of varnish removal from easel paintings," Microchem. J. 138, 7-18 (2018).
- 26. S. Song, J. Xu, and R. K. Wang, "Long-range and wide field of view optical coherence tomography for in vivo 3D imaging of large volume object based on akinetic programmable swept source," Biomed. Opt. Express 7, 4734-4748 (2016).
- 27. F. Zaki, I. Hou, D. Cooper, D. Patel, Y. Yang, and X. Liu, "Highdefinition optical coherence tomography imaging for noninvasive examination of heritage works," Appl. Opt. 55, 10313-10317 (2016).
- 28. X. Liu, Y. Huang, and J. U. Kang, "Distortion-free freehandscanning OCT implemented with real-time scanning speed variance correction," Opt. Express 20, 16567-16583 (2012).
- 29. K. Zhang, W. Wang, J. Han, and J. U. Kang, "A surface topology and motion compensation system for microsurgery guidance and intervention based on common-path optical coherence tomography," IEEE Trans. Biomed. Eng. 56, 2318-2321 (2009).